Cell Reports

Resource

Quantitative and Dynamic Catalogs of Proteins Released during Apoptotic and Necroptotic Cell Death

Graphical Abstract

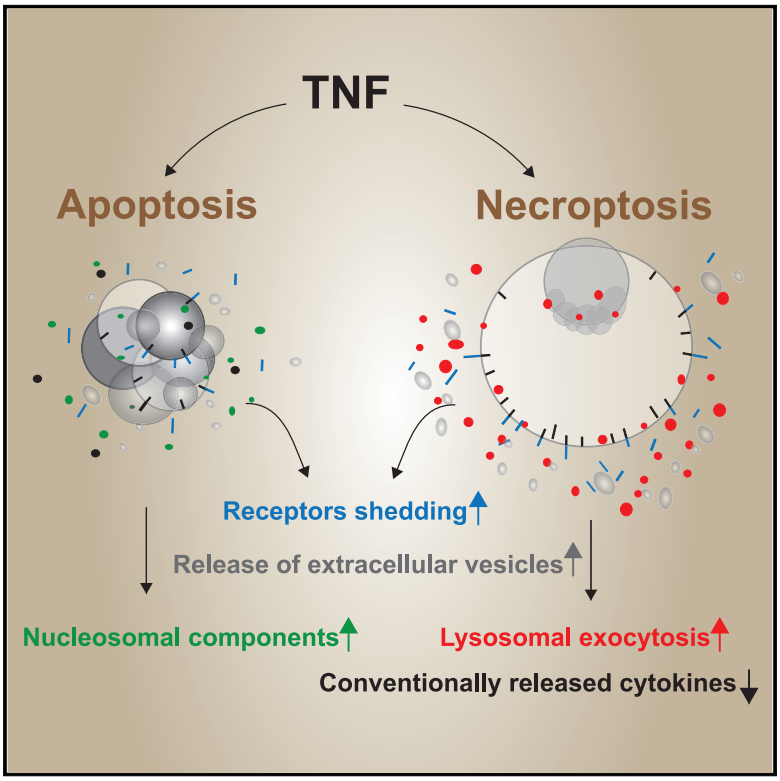

Highlights

- The release of conventionally secreted cytokines is reduced in necroptotic cells
- Receptor shedding occurs during TNF-induced necroptosis and apoptosis
- Lysosomal components are released via lysosomal exocytosis during necroptosis

Authors

Maria C. Tanzer, Annika Frauenstein, Che A. Stafford, Kshiti Phulphagar, Matthias Mann, Felix Meissner

Correspondence

mmann@biochem.mpg.de (M.M.), meissner@biochem.mpg.de (F.M.)

In Brief

Tanzer et al. provide a view of dynamically released proteins during TNF-induced apoptosis and necroptosis. The data highlight processes that are commonly and differentially regulated during these two different types of cell death.

Tanzer et al., 2020, Cell Reports *30*, 1260–1270
January 28, 2020
https://doi.org/10.1016/j.celrep.2019.12.079

CellPress

OPEN ACCESS
CellPress

Cell Reports
Resource

Quantitative and Dynamic Catalogs of Proteins Released during Apoptotic and Necroptotic Cell Death

Maria C. Tanzer,[1] Annika Frauenstein,[2] Che A. Stafford,[3] Kshiti Phulphagar,[2] Matthias Mann,[1,*] and Felix Meissner[2,4,*]
[1]Department of Proteomics and Signal Transduction, Max Planck Institute of Biochemistry, 82152 Martinsried, Germany
[2]Experimental Systems Immunology, Max Planck Institute of Biochemistry, 82152 Martinsried, Germany
[3]Gene Center and Department of Biochemistry, Ludwig-Maximilians-Universität, 81377 Munich, Germany
[4]Lead Contact
*Correspondence: mmann@biochem.mpg.de (M.M.), meissner@biochem.mpg.de (F.M.)
https://doi.org/10.1016/j.celrep.2019.12.079

SUMMARY

The inflammatory functions of the cytokine tumor necrosis factor (TNF) rely on its ability to induce cytokine production and to induce cell death. Caspase-dependent and caspase-independent pathways—apoptosis and necroptosis, respectively—regulate immunogenicity by the release of distinct sets of cellular proteins. To obtain an unbiased, systems-level understanding of this important process, we here applied mass spectrometry-based proteomics to dissect protein release during apoptosis and necroptosis. We report hundreds of proteins released from human myeloid cells in time course experiments. Both cell death types induce receptor shedding, but only apoptotic cells released nucleosome components. Conversely, necroptotic cells release lysosomal components by activating lysosomal exocytosis at early stages of necroptosis-induced membrane permeabilization and show reduced release of conventionally secreted cytokines.

INTRODUCTION

Tumor necrosis factor (TNF) is a major contributor to many inflammatory diseases, including psoriasis, rheumatoid arthritis, and inflammatory bowel disease (Bradley, 2008). This has initially been linked to TNF-induced production of various cytokines via nuclear factor κB (NF-κB) and mitogen-activated protein kinase (MAPK) pathway activation (Bradley, 2008). Subsequent reports, however, revealed a major role of TNF-induced cell death in inflammatory diseases (Rock and Kono, 2008). Binding of TNF to its receptor TNF-R1 activates the NF-κB and MAPK pathways, leading to cytokine production. Cellular inhibitor of apoptosis 1 and 2 (cIAP1 and cIAP2) regulate the activation of these pathways via their E3 ubiquitin ligase activity toward receptor-interacting serine/threonine-protein kinase 1 (RIPK1) (Bertrand et al., 2008). Inhibition of cIAPs using small molecules called Smac mimetics (SMs) results in decreased NF-κB signaling and caspase-8 activation (Arslan and Scheidereit, 2011; Vince et al., 2007; Varfolomeev et al., 2007). This triggers the activation of downstream caspases and initiates the apoptotic process, which involves nuclear fragmentation, blebbing, and cell shrinkage (Elmore, 2007). During the early stages of apoptosis, phosphatidylserine is exposed on the cell surface, which is recognized by macrophages that engulf dying cells (Fadok et al., 1992). Although released histones have been described to activate Toll-like receptors and induce cytokine production, apoptosis is conceptually considered an immunological silent death (Elliott and Ravichandran, 2010).

Caspase inhibition prevents apoptosis, but in many cell types it triggers an alternative cell death pathway termed necroptosis (Vercammen et al., 1998). Upon TNF signaling, caspase-8 regulates necroptosis by cleaving RIPK1 (Oberst et al., 2011; Pop et al., 2011). Caspase-8 inhibition leads to autophosphorylation and activation of RIPK1 and RIPK3. Active RIPK3 phosphorylates and activates the pseudokinase mixed lineage kinase domain-like protein (MLKL) (Murphy et al., 2013; Wang et al., 2014; Tanzer et al., 2017). Active MLKL translocates to the plasma membrane to induce membrane rupture (Hildebrand et al., 2014; Sun et al., 2012). Necroptosis is primarily thought of as an immunologically reactive process, because of its fast kinetics, the release of damage-associated molecular patterns (DAMPs) such as high mobility group box 1 protein (HMGB1) and ATP, as well as reduced macrophage engulfment (Kaczmarek et al., 2013).

Different modes of cell death can lead to significantly different physiological outcomes through the release of distinct molecules. For example, it was recently reported that necroptotic cell death in contrast to apoptotic cell death can drive a systemic immune response, leading to tumor regression (Snyder et al., 2019). The same group showed that cytokine mRNA translation continues at the endoplasmic reticulum (ER) during necroptosis even after plasma membrane rupture (Orozco et al., 2019). Another study reported that the cell death-dependent cytokine microenvironment determines the lineage commitment and thereby the harmfulness of hepatic cancer (Seehawer et al., 2018). Other studies compared the ability of cytokine and chemokine release by apoptotic and necroptotic cells (Kearney et al., 2015; Zhu et al., 2018). However, whereas Kearney et al. (2015) observed a decrease in cytokines released by necroptotic cells, Zhu et al. (2018) reported an activation of pro-inflammatory

cytokine gene expression instead. Together these studies underline the different properties of apoptotic and necroptotic cells on their surrounding microenvironment, which would now make it attractive to systematically investigate the released cellular contents.

Mass spectrometry-based proteomics has matured remarkably in recent years and now provides a comprehensive discovery tool to address diverse biological questions (Aebersold and Mann, 2016; Larance and Lamond, 2015). Here we set out to identify proteins released by apoptotic versus necroptotic cell death programs using a proteomics strategy we developed recently for the sensitive detection of secreted proteins (Meissner et al., 2013; Frauenstein and Meissner, 2018).

We induced TNF-mediated apoptosis and necroptosis in a lymphoma cell line and human primary macrophages. Proteomic analysis of supernatants and of enriched extracellular vesicles shed light on processes regulated during necroptosis and apoptosis and the cell death type-specific release of cytokines.

RESULTS

Differential Release of Proteins in Cells Undergoing TNF-Induced Apoptosis and Necroptosis

To define the inflammatory potential of apoptosis and necroptosis on a global scale, we set out to identify proteins released by cells undergoing TNF-mediated apoptosis or necroptosis. We induced both forms of cell death in the histiocytic lymphoma cell line U937 and in human primary macrophages, two cell types frequently used to investigate these cell death pathways (Tanzer et al., 2015; McComb et al., 2012) (Figure 1A). Apoptosis was triggered by TNF and the SM birinapant, while the further addition of the caspase inhibitor IDUN-6556 (IDN-6556) led to necroptosis. Both processes showed similar kinetics when comparing caspase cleavage (Figure 1B), a hallmark of apoptosis, with phosphorylation of MLKL (Figure 1C), a hallmark of necroptosis. During necroptosis, activated MLKL translocates to the plasma membrane and leads to immediate membrane permeabilization and propidium iodide intake (Hildebrand et al., 2014), whereas apoptotic cells retain plasma membrane integrity until the later stages when secondary necrosis occurs (Figure 1D; Figure S1A). A recent report showed that active caspase-8 can cleave gasdermin-D, a pore-forming protein that induces plasma membrane rupture during pyroptosis (Orning et al., 2018). We cannot exclude processing of gasdermin-D at later time points of apoptosis. Nevertheless, the slow kinetics and reduced level of propidium iodide intake (Figure 1D) and the delayed release of HMGB1 (Figures S2B and S2C) (a prominent marker of necroptosis and pyroptosis; Kaczmarek et al., 2013) are strong indications against a potential involvement of pyroptosis upon TNF and SM stimulation, at least before secondary necrosis.

To analyze proteins released by apoptotic and necroptotic cells, supernatants were harvested and digested, and the resulting peptides were directly analyzed by single-run liquid chromatography mass spectrometry (LC-MS/MS) coupled to high-resolution mass spectrometry on the quadrupole Orbitrap analyzer (STAR Methods; Figure 1A). Label-free quantification of the MS data and statistical analysis were performed using MaxQuant and Perseus (Cox and Mann, 2008; Tyanova et al., 2016). Overall, 3,507 proteins were identified from U937 supernatants, with an average of 2,058 protein groups per sample (Figure 1E). Principal-component analysis revealed partial stimulation and time-dependent separation of samples (Figures S1B and S1C). Necroptotic supernatants from later time points, when membrane permeabilization occurred, separated from the rest of the samples (Figures S1B and S1C). Consistently, the levels of hundreds of proteins were significantly changed in the supernatants of necroptotic cells, compared with control samples (Figure 1F). In contrast, this was the case for only 34 proteins in apoptosis. However, at a later time point apoptotic cells, which undergo secondary necrosis, also significantly released several hundreds of proteins (Figure S1D). The fold changes of all proteins measured across seven apoptotic and four necroptotic time points compared with respective controls are provided in Table S1. When we analyzed the proteome of the dying cells, the most apparent variation in protein levels occurred in necroptotic cells, including a reduction in cytosolic proteins, and an increase in mitochondrial proteins and proteins located at the ER (Figure S1E).

The Release of Conventionally Secreted Cytokines Is Significantly Reduced in Necroptotic Cells

TNF induces the production of a wide range of cytokines required to fight infection, and we were particularly interested in the effect of TNF-induced cell death on their release. CCL2 and IL8 were most strongly induced through TNF stimulation in U937 cells (Figures 2A and 2B), looking at all cytokines (retrieved from the keyword annotation "Cytokines"; STAR Methods). At later time points, levels of CCL2 and IL8 were diminished in supernatants of apoptotic cells, but this was not statistically significant. However, we observed a significant downregulation for both cytokines during necroptosis compared with TNF-only treatment. To confirm our mass spectrometry results, we used enzyme-linked immunosorbent assay (ELISA) to measure levels of CCL2 and HMGB1 in supernatants, which showed a similar trend (Figures S2A–S2C). CCL2 and IL8 contain an N-terminal signal peptide and are therefore part of the keyword annotation "Signal" (hereafter referred to as signal proteins). The signal peptide mediates conventional secretion through the ER-Golgi secretory pathway. Other conventionally secreted cytokines were also downregulated at later stages of necroptosis in U937 cells (Figure S2D) and primary macrophages (Figures 2C and 2D; Figure S2E). Levels of most non-conventionally released cytokines were primarily unaffected or increased in necroptotic supernatants because of membrane permeabilization (Figure S2F). AIMP-1 levels, for example, were enriched in a minor but significant way in necroptotic supernatants (Figure S2F).

We examined the release of all conventionally released proteins to test whether the secretion of the ER-Golgi network is generally affected by necroptosis. Surprisingly, we detected an increased release of signal proteins at 3 h of necroptosis treatment (Figure 2E; Figure S2G), while intracellular levels of

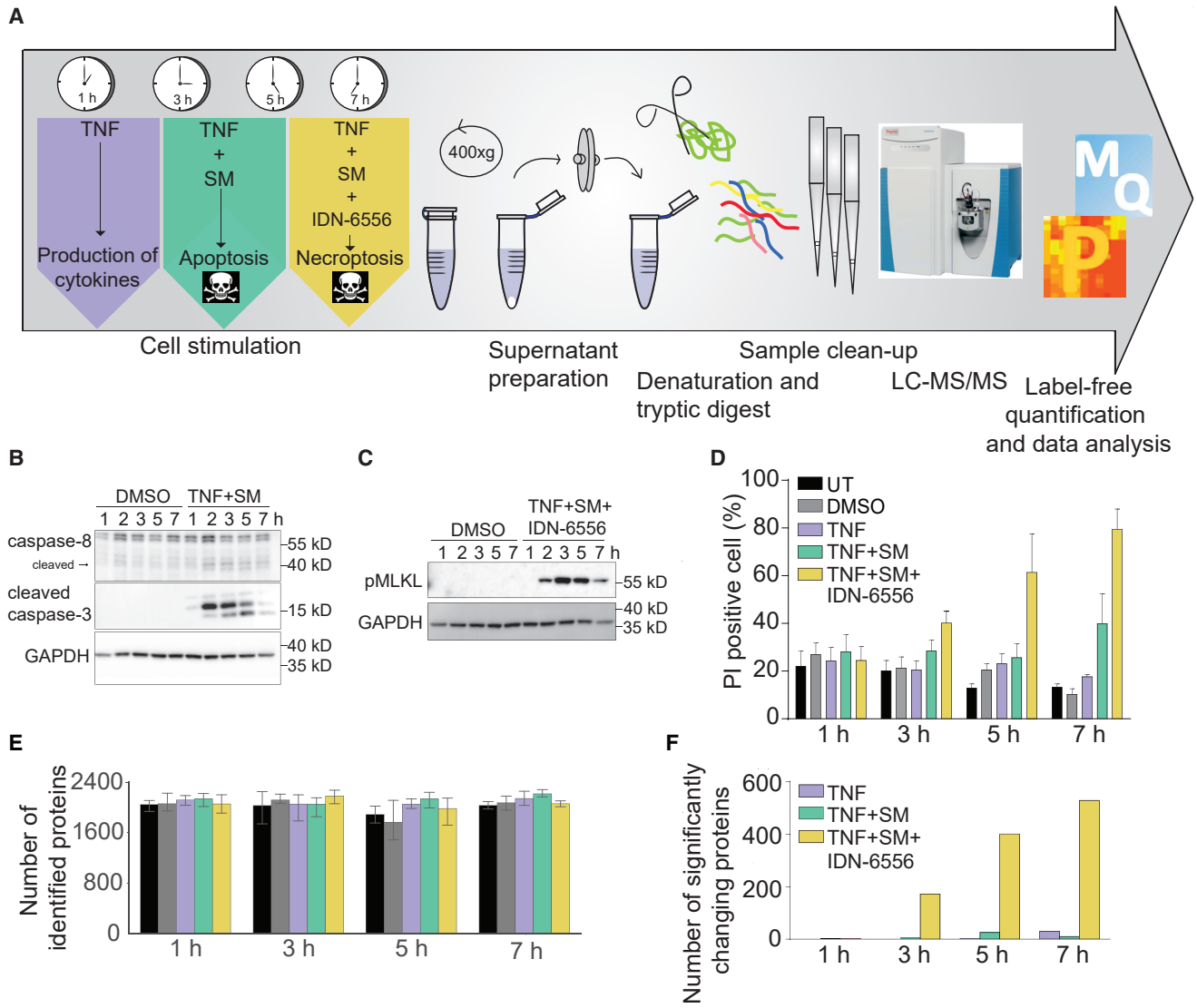

Figure 1. Supernatant Analysis of Cells Undergoing TNF-Induced Apoptosis and Necroptosis

(A) Schematic workflow of supernatant processing.

(B and C) Immunoblot of U937 cells treated with DMSO, TNF (30 ng/mL), and SM (birinapant, 250 nM) to induce apoptosis or with TNF, SM, and IDN-6556 (IDN-6556, 10 μM) to induce necroptosis for 1–7 h and blotted for the apoptotic markers cleaved caspase-8 and caspase-3 (B) and the necroptotic marker phosphorylated MLKL (C) and the loading control GAPDH.

(D) Cell death analysis by flow cytometry of propidium iodide-positive cells, which were treated as indicated over a time course of 1–7 h (±SEM, n = 3 or 4).

(E) Number of all proteins quantified in the supernatant of cells treated as indicated in (D).

(F) Number of significantly changing proteins in supernatants of cells treated as indicated (Student's t test: false discovery rate [FDR] = 0.05).

the same proteins were unaffected (Figure S2H). Proteins that are unconventionally secreted (assigned to the keyword annotation "Secreted", excluding signal proteins) were not changed in the supernatant of necroptotic cells (Figure 2E). The release of conventionally released proteins at 3 h of stimulation was most strongly inhibited in necroptotic cells by brefeldin A treatment (Figure 2F), which leads to disruption of the Golgi apparatus. This indicates that the ER-Golgi secretory pathway is activated at early stages of necroptosis.

However, at 5 (Figures S2I and S2J) and 7 h of stimulation (Figure 2G) we detected fewer signal proteins in supernatants of necroptotic cells compared with the control treated cells, while intracellular levels were again unaffected (Figure S2K). This corresponds to the missing impact of brefeldin A on the signal protein level in supernatants of necroptotic cells treated for 7 h (Figure 2H). To determine whether degradation of signal proteins occurs because of an increased release of proteases at later stages of necroptosis, we analyzed semi-tryptic peptides of those proteins. Semi-tryptic peptides are generated by proteolytic processing prior to the proteomic workflow. In necroptotic supernatants at 7 h of necroptosis induction semi-tryptic peptides of signal proteins are slightly

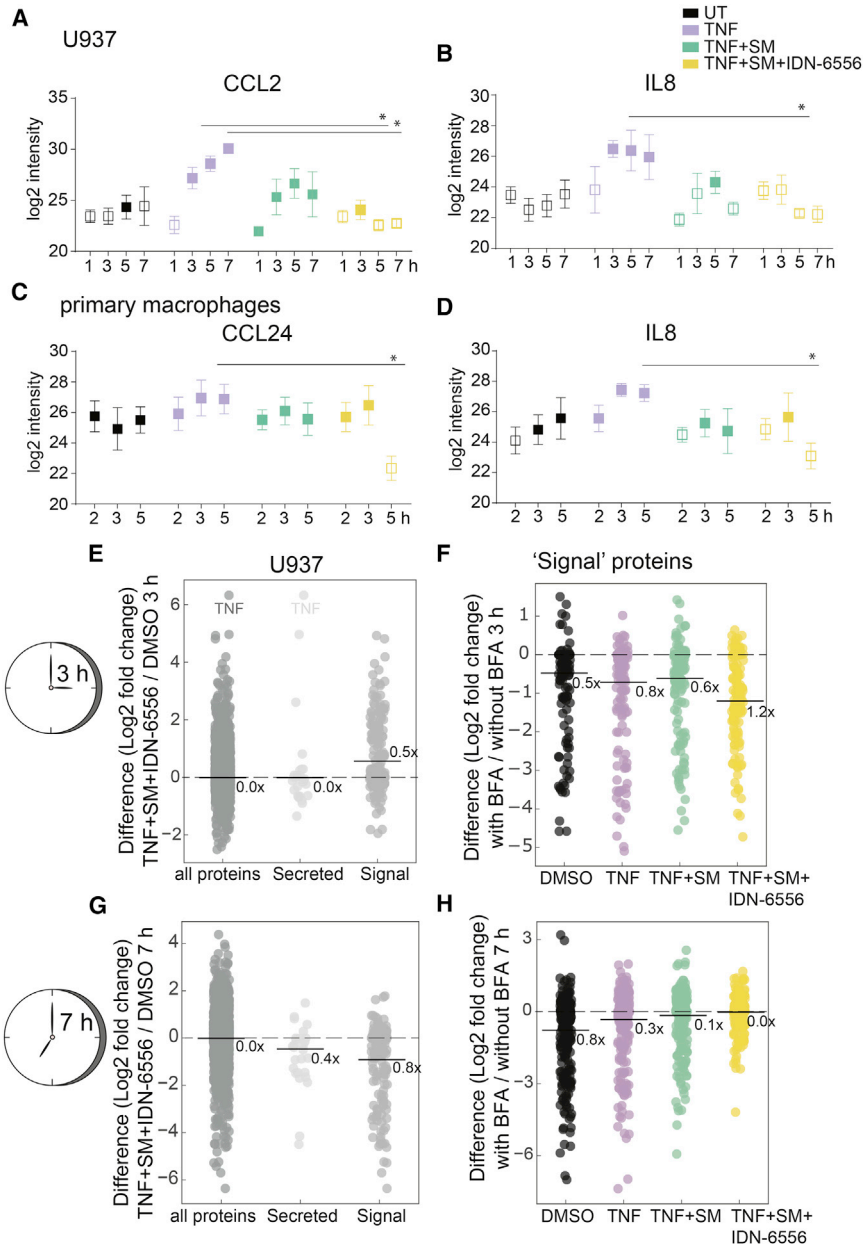

Figure 2. The Release of Conventionally Secreted Cytokines Is Reduced in Necroptotic Cells

(A–D) Graphs show the $\log_2$ intensity of CCL2 and IL8 in supernatants of U937 cells (A and B) and CCL24 and IL8 in supernatants of primary macrophages (C and D) measured using mass spectrometry. Cells were either left untreated (black squares) or treated with TNF (purple squares), TNF and SM (green squares), or TNF, SM, and IDN-6556 (yellow squares) over a time course of 1–7 h (for U937 cells) and 2–5 h (for primary macrophages) (±SEM, n = 3 or 4). Full squares represent two or more valid values for the data point. Asterisks show significant changes (Student's t test: FDR = 0.05).

(E and G) Swarm plot showing $\log_2$ fold change of all proteins (dark gray) and proteins assigned to the keyword annotation "Secreted" (all proteins annotated to the keyword annotation "Signal" were excluded, light gray, 1D annotation, not significant [n.s.], E, $p = 1.8 \times 10^{-4}$, G) and "Signal" (gray, $p = 2.1 \times 10^{-6}$, E, $p = 2.8 \times 10^{-21}$, G) released by necroptotic cells compared with the DMSO control at 3 h (E) and 7 h (G) of treatment. Taking the antilogarithm, we obtain fold changes of the mean protein distributions (x for fold). Fold changes above 0 represent enrichment and fold changes below 0 represent de-enrichment.

(F and H) Swarm plot showing $\log_2$ fold change of as "Signal" annotated proteins of U937 cells treated with brefeldin A (BFA; 5 μg/mL) and DMSO (black; $p = 1.1 \times 10^{-27}$, F, $p = 1.9 \times 10^{-8}$, H), TNF (purple; $p = 1.5 \times 10^{-36}$, F, n.s., H), TNF and SM (green; $p = 5.8 \times 10^{-26}$, F, n.s., H), or TNF, SM, and IDN-6556 (yellow; $p = 1.8 \times 10^{-35}$, F, n.s., H) compared with the same treatments without brefeldin A.

increased compared with the same peptides in necroptotic supernatants at 3 h of stimulation (Figure S2L). However, no semi-tryptic peptide of the conventionally released cytokines CCL2, IL8, and GRN could be detected. Necroptotic supernatants contained primarily semi-tryptic peptides of other proteins than signal proteins (Figure S2L), suggesting that the reduction of conventionally released proteins in supernatants of late-stage necroptotic cells is not only due to increased proteolytic processing. This indicates that the ER-Golgi secretory pathway is inhibited at later stages of necroptosis.

Although the inhibition of the ER-Golgi pathway at later stages of necroptosis prevents the release of conventionally released cytokines, TNF-induced cytokines CCL2 and IL8 levels were already reduced at 3 h of stimulation compared with TNF treatment alone. To test whether CCL2 is transcribed in response to TNF during necroptosis, we measured its mRNA levels and found a strong reduction compared with TNF-only treated cells after 3 and 7 h of stimulation (Figure S2M). The expression of other TNF-induced genes in U937 cells was also compromised. Of six proteins strongly upregulated in response to TNF treatment, we only found SOD2 being upregulated during necroptosis (Figure S2N). SQSTM1, NFKB2, ICAM1, PLAU, and JUND, which are all prominent targets of TNF, were not induced during necroptosis.

Receptor Shedding Occurs in Necroptotic and Apoptotic Cells

Comparing proteins released by necroptotic supernatants and apoptotic cells, we identified several proteins assigned to the keyword annotations "Receptor" as most enriched in both supernatants (Figures 3A–3C; Figure S3A; Table S2). This is unlikely to be a consequence of passive protein release caused by membrane damage, as necroptosis and apoptosis

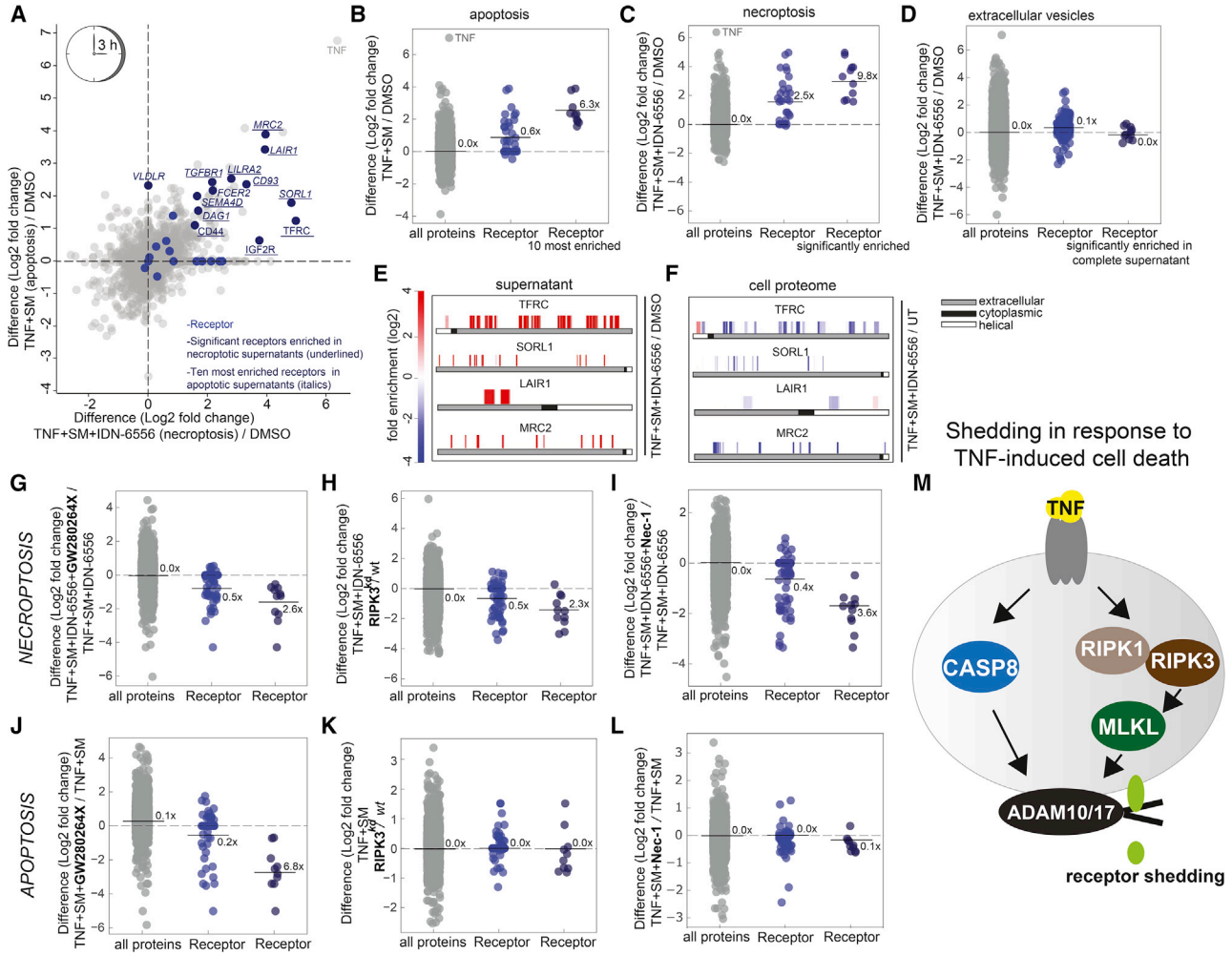

Figure 3. Necroptosis and Apoptosis Induce Receptor Shedding Mediated by ADAMs

(A) Scatterplot plotting the $\log_2$ fold change of proteins released by necroptotic cells compared with the DMSO control against the fold change of proteins released by apoptotic cells compared with the DMSO control (3 h of treatment). Proteins assigned to the keyword annotation "Receptor" (blue), ten most enriched receptors in apoptotic supernatants (dark blue, italics), and most significant receptors in necroptotic supernatants (dark blue, underlined).

(B) Swarm plot showing $\log_2$ fold change of all proteins (gray) and proteins assigned to the keyword annotation "Receptor" (blue; $p = 2.6 \times 10^{-6}$) released by apoptotic cells compared with the DMSO control at 3 h of treatment.

(C) Swarm plot showing $\log_2$ fold change of all proteins (gray) and "Receptor" proteins (blue; $p = 1.3 \times 10^{-7}$) released by necroptotic cells compared with the DMSO control at 3 h of treatment.

(D) Swarm plot showing $\log_2$ fold change of all proteins (gray), receptors (blue; n.s.), and significantly upregulated receptors in the supernatant of necroptotic cells (dark blue) present in extracellular vesicles of necroptotic cells compared with the DMSO control at 3 h of treatment.

(E and F) Matching of detected peptides by mass spectrometry to corresponding proteins using R shows peptide fold changes ($\log_2$) in the supernatant (E) and the cellular proteome (F) of necroptotic U937 cells at 3 h of stimulation compared with DMSO-treated control cells. Selected proteins are the four most enriched receptors in the supernatant of necroptotic U937 cells compared with the DMSO control. Values are averages of n = 4.

(G) Swarm plot showing $\log_2$ fold change of all proteins (gray), receptors (blue; $p = 6.8 \times 10^{-13}$), and significantly upregulated receptors in the supernatant of necroptotic cells (dark blue) present in supernatants of cells treated with TNF, SM, and IDN-6556 and the ADAM inhibitor GW280264X compared with cells treated with TNF, SM, and IDN-6556 for 3 h.

(H) Swarm plot showing $\log_2$ fold change of all proteins (gray), receptors (blue; $p = 3.0 \times 10^{-3}$, FDR = 0.1), and significantly upregulated receptors in the supernatant of necroptotic cells (dark blue) present in supernatants of cells deficient for RIPK3 treated with TNF, SM, and IDN-6556 compared with wild-type cells treated the same for 3 h.

(I) Swarm plot showing $\log_2$ fold change of all proteins (gray), receptors (blue; $p = 0.001$), and significantly upregulated receptors in the supernatant of necroptotic cells (dark blue) present in supernatants of cells treated with TNF, SM, IDN-6556, and the RIPK1 inhibitor necrostatin-1 (Nec-1) compared with cells treated with TNF, SM, and IDN-6556 for 3 h.

(J) Swarm plot showing $\log_2$ fold change of all proteins (gray), receptors (blue; $p = 1.4 \times 10^{-6}$), and the ten most enriched receptors in the supernatants of apoptotic cells (dark blue) present in supernatants of cells treated with TNF, SM, and the ADAM inhibitor GW280264X compared with cells treated with TNF and SM for 3 h.

(legend continued on next page)

induction at 3 h precedes membrane permeabilization (Figure 1D). To test whether the detected receptors are instead released via exocytosis, we purified extracellular vesicles using serial centrifugation (STAR Methods). Proteomic analysis, however, showed no enrichment for receptors in extracellular vesicles of necroptotic and apoptotic cells compared with the control (Figure 3D; Figure S3B). Next, we sought to determine whether ectodomains are cleaved off the receptors and therefore enriched in necroptotic supernatants. Indeed, peptides derived from receptor ectodomains were preferentially released into the supernatant, whereas transmembrane or cytoplasmic domain peptides were either not detected or not enriched compared with supernatants of DMSO-treated cells (Figure 3E; Figure S3C). These cytoplasmic regions were readily detected when measuring the cellular proteome (Figure 3F; Figure S3D). A recent study showed that shedding during necroptosis contributes to inflammation and cell death in an MLKL-dependent manner (Cai et al., 2016). We show here that shedding also occurs to a lesser degree in apoptotic cells. Western blot analysis on the cell lysates did not detect phosphorylated/active MLKL at any time points during apoptosis induction, ruling out the possibility that necroptotic cells were present during apoptotic stimulation (Figure S4E).

Next, we tested whether this shedding is mediated via A disintegrin and metalloproteinase 10 (ADAM10) and 17, which are members of the disintegrins and metalloproteinase family (Cai et al., 2016). Indeed, specific inhibition of ADAM17 and ADAM10 with GW280264X reduced the release of receptors in necroptotic as well as apoptotic cells, while the release of proteins without receptor annotations remained unchanged (Figures 3G and 3J).

The lack of motif specificity for ADAM substrates complicates substrate prediction (Gooz, 2010), and we wished to investigate if there was a relationship between receptor abundance and receptor shedding. From the proteomic analysis of receptor levels in untreated cells, we conclude that the expression level itself has no impact on shedding (Figure S3F). Furthermore, the enrichment of shed receptors in the supernatant of necroptotic cells corresponded with their de-enrichment in these cells at 3 h after induction (Figure S3G).

Necroptosis-induced shedding was strongly inhibited in U937 cells deficient for RIPK3, the key activator of MLKL, or in U937 cells additionally treated with the RIPK1 inhibitor necrostatin-1 (Nec-1), where activation of MLKL cannot occur (Figures 3H and 3I; Figures S3H and S3I). In contrast to shedding during necroptosis, apoptosis-induced shedding was not prevented in RIPK3-deficient U937 cells or by addition of the RIPK1 inhibitor Nec-1 (Figures 3K and 3L). This indicates that TNF-induced shedding can be completely prevented only by blocking both caspase activation and the necroptotic pathway. Hence, we conclude that the shedding of receptors occurs during TNF-induced cell death and is not only restricted to necroptosis (Figure 3M).

Apoptotic Cells Exclusively Release Histones while Necroptotic Cells Release Lysosomal Proteins

We observed the release of apoptotic- and necroptotic-specific proteins. A group of proteins annotated as nucleosome components were most strongly enriched in supernatants of apoptotic cells (Figures 4A–4C; Figures S4A–S4C) at 3 h when DNA fragmentation and chromatin condensation were detected (Figures S4D and S4E). This was not the case in necroptosis, in which nucleosomes were de-enriched (Figure 4A; Figure S4F).

Necroptotic cells showed an increased release of lysosomal proteins after 3 h of necroptosis stimulation (Figures 4A and 4D; Figure S4G; Table S2), which was not evident during apoptosis. The release of lysosomal components was strongly reduced by the RIPK1 inhibitor Nec-1 and even more so in RIPK3-deficient U937 cells, suggesting a necroptosis-specific release pathway (Figures S4H and S4I).

Because many lysosomal proteins require cleavage for full activation, we examined whether the released lysosomal components are present in mature (cleaved) or premature (uncleaved) forms. Matching the peptide sequences to their proteins revealed that the majority were located within the mature forms of proteins released by necroptotic cells (Figure S4J). Consistently, we detected an increase of mature cathepsin B and cathepsin D in supernatants of necroptotic cells compared with DMSO-treated cells by immunoblotting (Figure S4K). Furthermore, we observed a significant increase of semi-tryptic peptides with comparable intensities to tryptic peptides of the same proteins in the supernatants of necroptotic cells (Figure S4L). Their near doubling (at 7 h) proves a dramatic increase of enzymatic activity in the supernatants of necroptotic cells. This is less likely due to increased ADAM activity, as they are active before and at 3 h of necroptosis induction. The numbers of all peptides identified across treatments did not significantly change (Figure S4M).

Membrane Permeabilization during Necroptosis Induces Lysosomal Exocytosis

Several studies have implicated the lysosomal machinery in necroptosis. The bursting of lysosomes within cells during necroptosis that preceded membrane permeabilization has been described (Vanden Berghe et al., 2010), and a role for MLKL in endosomal trafficking and increased vesicle formation has been reported (Yoon et al., 2017). Taking these studies into consideration, we asked whether lysosomal proteins were released via extracellular vesicles during exocytosis. Principal-component analysis revealed a clear separation of extracellular vesicle proteomes derived from apoptotic and necroptotic cells (Figure S4N). Consistent with previous reports, levels of MLKL and ESCRT proteins, which are involved in extracellular

(K) Swarm plot showing $\log_2$ fold change of all proteins (gray), receptors (blue; n.s.), and the ten most enriched receptors (dark blue) present in supernatants of cells deficient for RIPK3 treated with TNF and SM compared with wild-type cells treated the same for 3 h.
(L) Swarm plot showing $\log_2$ fold change of all proteins (gray), receptors (blue; $p = 2.0 \times 10^{-3}$, FDR = 0.1), and the ten most enriched receptors (dark blue) present in supernatants of cells treated with TNF, SM, and the RIPK1 inhibitor necrostatin-1 (Nec-1) compared with cells treated with TNF and SM for 3 hours.
(M) Scheme of receptor shedding downstream of apoptosis and necroptosis induction.

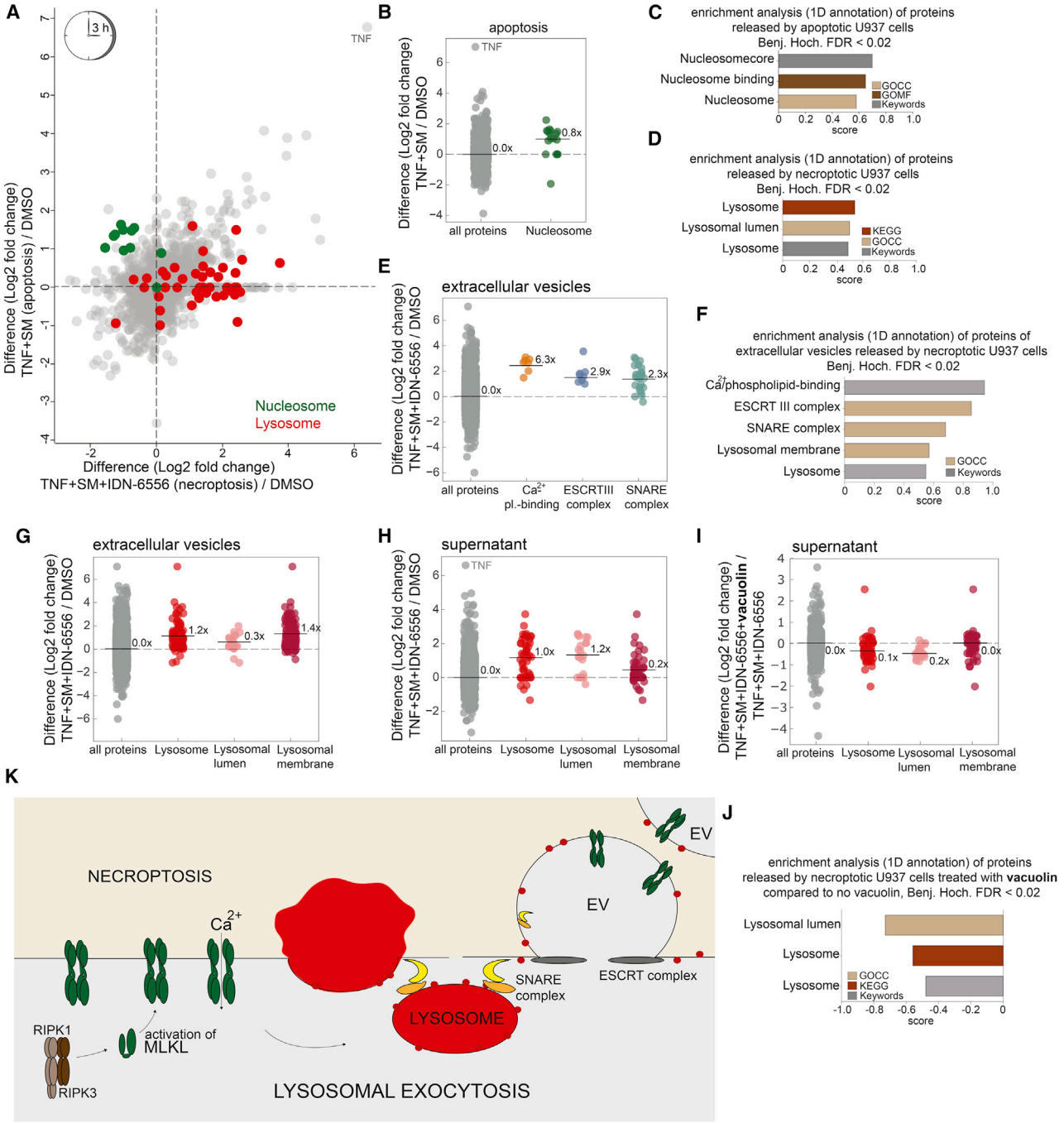

Figure 4. Lysosomal Proteins Are Released by Necroptotic Cells via Lysosomal Exocytosis

(A) Scatterplot plotting the $\log_2$ fold change of proteins released by necroptotic cells compared with the DMSO control against the fold change of proteins released by apoptotic cells compared with the DMSO control (3 h of treatment; "Nucleosome" [green], "Lysosome" [red]).

(B) Swarm plot showing $\log_2$ fold change of all proteins (gray) and proteins assigned to the GOCC annotation "Nucleosome" (green; $p = 1.2 \times 10^{-5}$) released by apoptotic cells compared with the DMSO control at 3 h of treatment.

(C and D) 1D annotation enrichment analysis of all proteins in the supernatant of apoptotic (C) and necroptotic (D) U937 cells treated for 3 h compared with the DMSO-treated control cells. Annotations including "Nucleosome" (C) and "Lysosome" (D) were selected and ranked from higher score to lower score (Benjamini-Hochberg FDR = 0.02) (STAR Methods). KEGG, Kyoto Encyclopedia of Genes and Genomes; GOCC, Gene Ontology cellular components; GOMF, Gene Ontology molecular function.

(E) Swarm plot showing $\log_2$ fold change of all proteins (gray) and proteins assigned to the annotation "Calcium/phospholipid binding" (keyword, yellow), the "ESCRTIII complex" (GOCC, blue), and "SNARE complex" (GOCC, green) present in extracellular vesicles of necroptotic cells compared with the DMSO control

(legend continued on next page)

vesicle formation and removal of MLKL from the plasma membrane, were increased in extracellular vesicles derived from necroptotic cells compared with control or apoptotic cells after 3 h of stimulation (Yoon et al., 2017; Gong et al., 2017) (Figures 4E and 4F; Figure S4O).

Interestingly, we observed a significant enrichment of lysosomal components in extracellular vesicles of necroptotic cells (Figures 4F and 4G; Figure S4O). Luminal lysosomal proteins were preferentially present in total supernatants, whereas membrane-bound ones were found mainly in purified extracellular vesicles (Figures 4H and 4G). Distribution of lysosomal membrane and lysosomal luminal proteins differed significantly ($p < 0.0001$). In classical endosomal exocytosis, luminal and membrane lysosomal proteins would be co-released in extracellular vesicles, which is not the case here.

An alternative process, termed lysosomal exocytosis, which occurs in response to plasma membrane permeabilization, for example, through ionomycin treatment or mechanical stress, has also been described in TNF-treated L929 cells, presumably to repair plasma membranes (Andrews, 2002; Reddy et al., 2001; Ono et al., 2001). In that process, the lysosomal membrane fuses with the plasma membrane, releasing its cargo into the extracellular space. This corresponds with our observation that luminal lysosomal proteins are enriched in the supernatant, and membrane lysosomal proteins are enriched in extracellular vesicles that also contain plasma membrane. Also the enrichment of calcium/phospholipid-binding and SNARE (SNAP receptor) proteins, which play an important role in vesicle fusion in response to increased intracellular free calcium upon membrane permeabilization, fits the model of lysosomal exocytosis. (Rao et al., 2004; Shen et al., 2016) (Figures 4E, 4F, and 4K; Figure S4O).

To determine the role of lysosomal exocytosis in the release of lysosomal components, we inhibited lysosomal exocytosis using vacuolin, which leads to homotypic fusion of endosomes and lysosomes. It blocks calcium-dependent exocytosis in a cell type-dependent manner (Cerny et al., 2004; Lu et al., 2014; Shaik et al., 2009). Treatment of necroptotic cells with vacuolin partially inhibited the release of lysosomal components in the total supernatant (Figures 4I and 4J).

DISCUSSION

Chronic inflammatory TNF-induced cell death is a major contributor to a range of inflammatory diseases, as dying cells expose immunogenic proteins normally found within the cell. Our proteomic approach provided a comprehensive and unbiased view on proteins released by apoptotic and necroptotic cells. As expected, many proteins were statistically significantly changed in supernatants of apoptotic cells compared with control. This was even more pronounced in necroptosis, particularly at later time points.

The release of pro-inflammatory cytokines contributes to the immunogenicity of cell death pathways. Whereas conventionally released cytokines were generally reduced in supernatants of necroptotic cells, non-conventionally released cytokines were primarily unchanged or increased compared with TNF alone or apoptosis. Plasma membrane permeabilization facilitates the unconventional release of cytokines. The reduction of conventionally released cytokines is due to the inhibition of the ER-Golgi trafficking pathway at later stages of necroptosis and the early plasma membrane permeabilization, which is most likely the reason for compromised transcription and expression of TNF-induced proteins. These findings do not conflict with the results of Orozco et al. (2019) regarding continuous cytokine mRNA translation despite plasma membrane permeabilization during necroptosis, because the cytokine production of stimulated living cells is expected to exceed that of necroptotic cells.

Other immunogenic proteins were differentially released by apoptotic and necroptotic cells, such as histones, which were increased only in supernatants of apoptotic cells. They are linked to diseases like lupus (Chen et al., 2014; Radic et al., 2004), chronic obstructive pulmonary disease (COPD), cerebral stroke, and sepsis. Conversely, HMGB1, a highly inflammatory molecule, was increased in the supernatants of necroptotic cells, as previously described (Magna and Pisetsky, 2014).

Besides the detection of proteins with known intercellular functions, our study provides insights into intracellular mechanisms that occur during TNF-induced cell death and that may also contribute to inflammation. For example, we observed an

at 3 h of treatment. The p value ($-\log_{10}$) of the 1D annotation enrichment for "Calcium/phospholipid binding" is 5.3×10^{-9}, for "ESCRTIII complex" is 2.9×10^{-5}, and for "SNARE complex" is 1.7×10^{-9}.

(F) 1D annotation enrichment analysis of all proteins of extracellular vesicles in the supernatant of necroptotic U937 cells treated for 3 h with TNF, SM, and IDN-6556 compared with the DMSO-treated control cells. Annotations are ranked from higher score to lower score (Benjamini-Hochberg FDR = 0.02).

(G) Swarm plot showing $\log_2$ fold change of all proteins (gray) and proteins assigned to the keyword annotations "Lysosome" (keywords, red), "Lysosomal lumen" (GOCC, nude), and "Lysosomal membrane" (GOCC, pink) in extracellular vesicles of necroptotic cells compared with the DMSO control at 3 h of treatment. The p value ($-\log_{10}$) of the 1D annotation enrichment for "Lysosome" is 3.8×10^{-23}, for "Lysosomal lumen" is 9.2×10^{-3} (FDR = 0.1), and for "Lysosomal membrane" is 2.7×10^{-29}.

(H) Swarm plot showing $\log_2$ fold change of the same annotation groups as in (G) released into the supernatant of necroptotic cells compared with the DMSO control at 3 h of treatment. The p value ($-\log_{10}$) of the 1D annotation enrichment for "Lysosome" is 1.6×10^{-10}, for "Lysosomal lumen" is 2.4×10^{-5}, and for "Lysosomal membrane" is 1.0×10^{-3}.

(I) Swarm plot showing $\log_2$ fold change of all proteins (gray) and lysosomal proteins (red) present in supernatants of cells treated with TNF, SM, IDN-6556, and the lysosomal exocytosis inhibitor vacuolin compared with cells treated with TNF, SM, and IDN-6556 for 3 h. The p value ($-\log_{10}$) of the 1D annotation enrichment for "Lysosome" is 9.8×10^{-12} and for "Lysosomal lumen" is 3.7×10^{-10}.

(J) 1D annotation enrichment analysis of all proteins in the supernatant of necroptotic U937 cells treated for 3 h with TNF, SM, IDN-6556, and vacuolin compared with the same treatment without vacuolin. Annotations containing "Lysosome" are selected and ranked from higher to lower score (Benjamini-Hochberg FDR = 0.02).

(K) Scheme of lysosomal exocytosis and formation of extracellular vesicle as response to plasma membrane permeabilization during necroptosis.

enrichment of receptor ectodomains in supernatants of necroptotic and apoptotic cells due to ADAM-mediated shedding. This is a physiologically important process: the cleavage of cell adhesion proteins promotes detachment of dying cells from surrounding tissue; receptor cleavage abrogates signal transduction into the cell as well as between cells by the generation of decoy receptors cleavage (Blaydon et al., 2011; Jones et al., 2016). Together, this switches signaling within dying cells to signaling between cells by the release of autocrine and paracrine signals. Shedding was already reported to be activated during necroptosis (Cai et al., 2016). Our data provide a catalog of proteins affected and demonstrate that it occurs at later stages of TNF-induced cell death and can be prevented only by inhibiting both apoptotic and necroptotic executioners. Further studies should delineate the intercellular activities of the distinct signals released by the different forms of cell death on neighboring cells.

A second unexpected group of proteins released by necroptotic cells belong to lysosomes. We conclude that this is caused by lysosomal fusion to the plasma membrane, a mechanism that results in the release of lysosomal cargo into the supernatant in response to membrane permeabilization, described as lysosomal exocytosis.

Lysosomal exocytosis was originally described as a plasma membrane repair mechanism in response to Ca^{2+} influx (Reddy et al., 2001). A study on the infection of pathogens with bacterial type III secretion system confirmed this role (Roy et al., 2004). During necroptosis the ESCRT machinery removes MLKL from the plasma membrane to prevent membrane permeabilization (Yoon et al., 2017; Gong et al., 2017). We speculate that lysosomal exocytosis is an additional and very last resort to protect the cell from death (Ono et al., 2001). Lysosomal exocytosis was also investigated as a defense mechanism to remove intracellular pathogens (Miao et al., 2015), but the effect of lysosomal enzymes on pathogens in the extracellular regions has not been studied in detail. Many lysosomal enzymes work best at acidic pH but may still retain some enzymatic activity in the extracellular space, which is sufficient to degrade the extracellular matrix (Fonović and Turk, 2014). This is consistent with our observation of increased semi-tryptic peptides in supernatants of necroptotic cells, which indicates increased proteolytic activity. These lysosomal enzymes may also affect cells in close proximity. Whether lysosomal exocytosis following necroptosis induction is just a consequence of cell membrane permeabilization or a last chance to rescue dying cells, and whether it significantly affects the environment, such as pathogens or neighboring cells, are exciting questions for future studies.

In conclusion, our study provides in-depth, quantitative, and dynamic catalogs of proteins differentially and commonly released during apoptotic and necroptotic cell death. This offers a solid basis for investigating the complexity of biological processes that are either incidental or regulated, harmful or functional during apoptosis and necroptosis. Our results demonstrate that an unexpectedly wide range of different proteins are released. Only some of these contribute directly to inflammation, whereas others are more likely to act in more complex ways that still need to be elucidated in detail in these very different modes of cell death.

STAR★METHODS

Detailed methods are provided in the online version of this paper and include the following:

- KEY RESOURCES TABLE
- LEAD CONTACT AND MATERIALS AVAILABILITY
- EXPERIMENTAL MODEL AND SUBJECT DETAILS
- METHOD DETAILS
  - Sample preparation for proteomic analysis and ELISA of supernatants
  - Preparation of extracellular vesicles
  - Western blotting
  - Cell death analysis
  - DNA laddering assay
  - qPCR
  - Chromatography and mass spectrometry
- QUANTIFICATION AND STATISTICAL ANALYSIS
- DATA AND CODE AVAILABILITY

SUPPLEMENTAL INFORMATION

Supplemental Information can be found online at https://doi.org/10.1016/j.celrep.2019.12.079.

ACKNOWLEDGMENTS

We thank James Murphy for critically reading the manuscript, Julie Stafford for proofreading, Georg H. Borner for his scientific input, and John Silke and Najoua Lalaoui (Walter and Eliza Hall Institute) for providing birinapant and compound A. Martin Spitaler, Giovanni Cardone, and Markus Oster (Max Planck Institute of Biochemistry) helped with flow cytometry. We also thank all members of the Department of Proteomics and Signal Transduction at the Max Planck Institute of Biochemistry in Martinsried for help and discussions, and especially Bianca Splettstoesser, Steven Dewitz, Igor Paron, Christian Deiml, and Gabriele Sowa for technical assistance. This work was supported by the Max Planck Society for the Advancement of Science Deutsche Forschungsgemeinschaft SFB914, and a Marie Skłodowska-Curie Actions Individual Fellowship to M.C.T.

AUTHOR CONTRIBUTIONS

M.C.T., M.M., and F.M. conceived the project and wrote the manuscript. M.M. and F.M. supervised the project. M.C.T. designed and performed all experiments and analyzed all data. A.F. helped with the preparation of human primary macrophages and modified the R script for peptide-to-protein matching. C.A.S. helped with western blotting and edited the manuscript. K.P. provided scientific input and edited the manuscript.

DECLARATION OF INTERESTS

The authors declare no competing interests.

Received: March 4, 2019
Revised: November 7, 2019
Accepted: December 19, 2019
Published: January 28, 2020

REFERENCES

Aebersold, R., and Mann, M. (2016). Mass-spectrometric exploration of proteome structure and function. Nature *537*, 347–355.

Andrews, N.W. (2002). Lysosomes and the plasma membrane: trypanosomes reveal a secret relationship. J. Cell Biol. *158*, 389–394.

Arslan, S.C., and Scheidereit, C. (2011). The prevalence of TNFα-induced necrosis over apoptosis is determined by TAK1-RIP1 interplay. PLoS ONE *6*, e26069.

Bertrand, M.J., Milutinovic, S., Dickson, K.M., Ho, W.C., Boudreault, A., Durkin, J., Gillard, J.W., Jaquith, J.B., Morris, S.J., and Barker, P.A. (2008). cIAP1 and cIAP2 facilitate cancer cell survival by functioning as E3 ligases that promote RIP1 ubiquitination. Mol. Cell *30*, 689–700.

Blaydon, D.C., Biancheri, P., Di, W.L., Plagnol, V., Cabral, R.M., Brooke, M.A., van Heel, D.A., Ruschendorf, F., Toynbee, M., Walne, A., et al. (2011). Inflammatory skin and bowel disease linked to ADAM17 deletion. N. Engl. J. Med. *365*, 1502–1508.

Bradley, J.R. (2008). TNF-mediated inflammatory disease. J. Pathol. *214*, 149–160.

Cai, Z., Zhang, A., Choksi, S., Li, W., Li, T., Zhang, X.M., and Liu, Z.G. (2016). Activation of cell-surface proteases promotes necroptosis, inflammation and cell migration. Cell Res. *26*, 886–900.

Cerny, J., Feng, Y., Yu, A., Miyake, K., Borgonovo, B., Klumperman, J., Meldolesi, J., McNeil, P.L., and Kirchhausen, T. (2004). The small chemical vacuolin-1 inhibits Ca(2+)-dependent lysosomal exocytosis but not cell resealing. EMBO Rep. *5*, 883–888.

Chen, R., Kang, R., Fan, X.G., and Tang, D. (2014). Release and activity of histone in diseases. Cell Death Dis. *5*, e1370.

Cox, J., and Mann, M. (2008). MaxQuant enables high peptide identification rates, individualized p.p.b.-range mass accuracies and proteome-wide protein quantification. Nat. Biotechnol. *26*, 1367–1372.

Cox, J., and Mann, M. (2012). 1D and 2D annotation enrichment: a statistical method integrating quantitative proteomics with complementary high-throughput data. BMC Bioinformatics *13* (*Suppl 16*), S12.

Cox, J., Neuhauser, N., Michalski, A., Scheltema, R.A., Olsen, J.V., and Mann, M. (2011). Andromeda: a peptide search engine integrated into the MaxQuant environment. J. Proteome Res. *10*, 1794–1805.

Elliott, M.R., and Ravichandran, K.S. (2010). Clearance of apoptotic cells: implications in health and disease. J. Cell Biol. *189*, 1059–1070.

Elmore, S. (2007). Apoptosis: a review of programmed cell death. Toxicol. Pathol. *35*, 495–516.

Fadok, V.A., Voelker, D.R., Campbell, P.A., Cohen, J.J., Bratton, D.L., and Henson, P.M. (1992). Exposure of phosphatidylserine on the surface of apoptotic lymphocytes triggers specific recognition and removal by macrophages. J. Immunol. *148*, 2207–2216.

Fonović, M., and Turk, B. (2014). Cysteine cathepsins and extracellular matrix degradation. Biochim. Biophys. Acta *1840*, 2560–2570.

Frauenstein, A., and Meissner, F. (2018). Quantitative proteomics of secreted proteins. Methods Mol. Biol. *1714*, 215–227.

Gong, Y.N., Guy, C., Olauson, H., Becker, J.U., Yang, M., Fitzgerald, P., Linkermann, A., and Green, D.R. (2017). ESCRT-III acts downstream of MLKL to regulate necroptotic cell death and its consequences. Cell *169*, 286–300.e16.

Gooz, M. (2010). ADAM-17: the enzyme that does it all. Crit. Rev. Biochem. Mol. Biol. *45*, 146–169.

Hildebrand, J.M., Tanzer, M.C., Lucet, I.S., Young, S.N., Spall, S.K., Sharma, P., Pierotti, C., Garnier, J.M., Dobson, R.C., Webb, A.I., et al. (2014). Activation of the pseudokinase MLKL unleashes the four-helix bundle domain to induce membrane localization and necroptotic cell death. Proc. Natl. Acad. Sci. U S A *111*, 15072–15077.

Jones, P., Côté, R.G., Cho, S.Y., Klie, S., Martens, L., Quinn, A.F., Thorneycroft, D., and Hermjakob, H. (2008). PRIDE: new developments and new datasets. Nucleic Acids Res. *36*, D878–D883.

Jones, J.C., Rustagi, S., and Dempsey, P.J. (2016). ADAM proteases and gastrointestinal function. Annu. Rev. Physiol. *78*, 243–276.

Kaczmarek, A., Vandenabeele, P., and Krysko, D.V. (2013). Necroptosis: the release of damage-associated molecular patterns and its physiological relevance. Immunity *38*, 209–223.

Kearney, C.J., Cullen, S.P., Tynan, G.A., Henry, C.M., Clancy, D., Lavelle, E.C., and Martin, S.J. (2015). Necroptosis suppresses inflammation via termination of TNF- or LPS-induced cytokine and chemokine production. Cell Death Differ. *22*, 1313–1327.

Kralj, M., Husnjak, K., Körbler, T., and Pavelić, J. (2003). Endogenous p21WAF1/CIP1 status predicts the response of human tumor cells to wild-type p53 and p21WAF1/CIP1 overexpression. Cancer Gene Ther. *10*, 457–467.

Larance, M., and Lamond, A.I. (2015). Multidimensional proteomics for cell biology. Nat. Rev. Mol. Cell Biol. *16*, 269–280.

Lu, Y., Dong, S., Hao, B., Li, C., Zhu, K., Guo, W., Wang, Q., Cheung, K.H., Wong, C.W., Wu, W.T., et al. (2014). Vacuolin-1 potently and reversibly inhibits autophagosome-lysosome fusion by activating RAB5A. Autophagy *10*, 1895–1905.

Magna, M., and Pisetsky, D.S. (2014). The role of HMGB1 in the pathogenesis of inflammatory and autoimmune diseases. Mol. Med. *20*, 138–146.

McComb, S., Cheung, H.H., Korneluk, R.G., Wang, S., Krishnan, L., and Sad, S. (2012). cIAP1 and cIAP2 limit macrophage necroptosis by inhibiting Rip1 and Rip3 activation. Cell Death Differ. *19*, 1791–1801.

Meissner, F., Scheltema, R.A., Mollenkopf, H.J., and Mann, M. (2013). Direct proteomic quantification of the secretome of activated immune cells. Science *340*, 475–478.

Miao, Y., Li, G., Zhang, X., Xu, H., and Abraham, S.N. (2015). A TRP channel senses lysosome neutralization by pathogens to trigger their expulsion. Cell *161*, 1306–1319.

Murphy, J.M., Czabotar, P.E., Hildebrand, J.M., Lucet, I.S., Zhang, J.G., Alvarez-Diaz, S., Lewis, R., Lalaoui, N., Metcalf, D., Webb, A.I., et al. (2013). The pseudokinase MLKL mediates necroptosis via a molecular switch mechanism. Immunity *39*, 443–453.

Nolte, H., MacVicar, T.D., Tellkamp, F., and Krüger, M. (2018). Instant Clue: a software suite for interactive data visualization and analysis. Sci. Rep. *8*, 12648.

Oberst, A., Dillon, C.P., Weinlich, R., McCormick, L.L., Fitzgerald, P., Pop, C., Hakem, R., Salvesen, G.S., and Green, D.R. (2011). Catalytic activity of the caspase-8-FLIP(L) complex inhibits RIPK3-dependent necrosis. Nature *471*, 363–367.

Ono, K., Wang, X., and Han, J. (2001). Resistance to tumor necrosis factor-induced cell death mediated by PMCA4 deficiency. Mol. Cell. Biol. *21*, 8276–8288.

Orning, P., Weng, D., Starheim, K., Ratner, D., Best, Z., Lee, B., Brooks, A., Xia, S., Wu, H., Kelliher, M.A., et al. (2018). Pathogen blockade of TAK1 triggers caspase-8-dependent cleavage of gasdermin D and cell death. Science *362*, 1064–1069.

Orozco, S.L., Daniels, B.P., Yatim, N., Messmer, M.N., Quarato, G., Chen-Harris, H., Cullen, S.P., Snyder, A.G., Ralli-Jain, P., Frase, S., et al. (2019). RIPK3 activation leads to cytokine synthesis that continues after loss of cell membrane integrity. Cell Rep. *28*, 2275–2287.e5.

Pop, C., Oberst, A., Drag, M., Van Raam, B.J., Riedl, S.J., Green, D.R., and Salvesen, G.S. (2011). FLIP(L) induces caspase 8 activity in the absence of interdomain caspase 8 cleavage and alters substrate specificity. Biochem. J. *433*, 447–457.

Radic, M., Marion, T., and Monestier, M. (2004). Nucleosomes are exposed at the cell surface in apoptosis. J. Immunol. *172*, 6692–6700.

Rao, S.K., Huynh, C., Proux-Gillardeaux, V., Galli, T., and Andrews, N.W. (2004). Identification of SNAREs involved in synaptotagmin VII-regulated lysosomal exocytosis. J. Biol. Chem. *279*, 20471–20479.

Reddy, A., Caler, E.V., and Andrews, N.W. (2001). Plasma membrane repair is mediated by Ca(2+)-regulated exocytosis of lysosomes. Cell *106*, 157–169.

Rock, K.L., and Kono, H. (2008). The inflammatory response to cell death. Annu. Rev. Pathol. *3*, 99–126.

Roy, D., Liston, D.R., Idone, V.J., Di, A., Nelson, D.J., Pujol, C., Bliska, J.B., Chakrabarti, S., and Andrews, N.W. (2004). A process for controlling

intracellular bacterial infections induced by membrane injury. Science *304*, 1515–1518.

Seehawer, M., Heinzmann, F., D'Artista, L., Harbig, J., Roux, P.F., Hoenicke, L., Dang, H., Klotz, S., Robinson, L., Doré, G., et al. (2018). Necroptosis microenvironment directs lineage commitment in liver cancer. Nature *562*, 69–75.

Shaik, G.M., Dráberová, L., Heneberg, P., and Dráber, P. (2009). Vacuolin-1-modulated exocytosis and cell resealing in mast cells. Cell. Signal. *21*, 1337–1345.

Shen, Y.T., Gu, Y., Su, W.F., Zhong, J.F., Jin, Z.H., Gu, X.S., and Chen, G. (2016). Rab27b is involved in lysosomal exocytosis and proteolipid protein trafficking in oligodendrocytes. Neurosci. Bull. *32*, 331–340.

Snyder, A.G., Hubbard, N.W., Messmer, M.N., Kofman, S.B., Hagan, C.E., Orozco, S.L., Chiang, K., Daniels, B.P., Baker, D., and Oberst, A. (2019). Intratumoral activation of the necroptotic pathway components RIPK1 and RIPK3 potentiates antitumor immunity. Sci. Immunol. *4*, eaaw2004.

Sun, L., Wang, H., Wang, Z., He, S., Chen, S., Liao, D., Wang, L., Yan, J., Liu, W., Lei, X., and Wang, X. (2012). Mixed lineage kinase domain-like protein mediates necrosis signaling downstream of RIP3 kinase. Cell *148*, 213–227.

Tanzer, M.C., Tripaydonis, A., Webb, A.I., Young, S.N., Varghese, L.N., Hall, C., Alexander, W.S., Hildebrand, J.M., Silke, J., and Murphy, J.M. (2015). Necroptosis signalling is tuned by phosphorylation of MLKL residues outside the pseudokinase domain activation loop. Biochem. J. *471*, 255–265.

Tanzer, M.C., Khan, N., Rickard, J.A., Etemadi, N., Lalaoui, N., Spall, S.K., Hildebrand, J.M., Segal, D., Miasari, M., Chau, D., et al. (2017). Combination of IAP antagonist and IFNγ activates novel caspase-10- and RIPK1-dependent cell death pathways. Cell Death Differ. *24*, 481–491.

Tyanova, S., Temu, T., Sinitcyn, P., Carlson, A., Hein, M.Y., Geiger, T., Mann, M., and Cox, J. (2016). The Perseus computational platform for comprehensive analysis of (prote)omics data. Nat. Methods *13*, 731–740.

Vanden Berghe, T., Vanlangenakker, N., Parthoens, E., Deckers, W., Devos, M., Festjens, N., Guerin, C.J., Brunk, U.T., Declercq, W., and Vandenabeele, P. (2010). Necroptosis, necrosis and secondary necrosis converge on similar cellular disintegration features. Cell Death Differ. *17*, 922–930.

Varfolomeev, E., Blankenship, J.W., Wayson, S.M., Fedorova, A.V., Kayagaki, N., Garg, P., Zobel, K., Dynek, J.N., Elliott, L.O., Wallweber, H.J., et al. (2007). IAP antagonists induce autoubiquitination of c-IAPs, NF-kappaB activation, and TNFalpha-dependent apoptosis. Cell *131*, 669–681.

Vercammen, D., Beyaert, R., Denecker, G., Goossens, V., Van Loo, G., Declercq, W., Grooten, J., Fiers, W., and Vandenabeele, P. (1998). Inhibition of caspases increases the sensitivity of L929 cells to necrosis mediated by tumor necrosis factor. J. Exp. Med. *187*, 1477–1485.

Vince, J.E., Wong, W.W., Khan, N., Feltham, R., Chau, D., Ahmed, A.U., Benetatos, C.A., Chunduru, S.K., Condon, S.M., McKinlay, M., et al. (2007). IAP antagonists target cIAP1 to induce TNFalpha-dependent apoptosis. Cell *131*, 682–693.

Wang, H., Sun, L., Su, L., Rizo, J., Liu, L., Wang, L.F., Wang, F.S., and Wang, X. (2014). Mixed lineage kinase domain-like protein MLKL causes necrotic membrane disruption upon phosphorylation by RIP3. Mol. Cell *54*, 133–146.

Yoon, S., Kovalenko, A., Bogdanov, K., and Wallach, D. (2017). MLKL, the protein that mediates necroptosis, also regulates endosomal trafficking and extracellular vesicle generation. Immunity *47*, 51–65.e7.

Zhu, K., Liang, W., Ma, Z., Xu, D., Cao, S., Lu, X., Liu, N., Shan, B., Qian, L., and Yuan, J. (2018). Necroptosis promotes cell-autonomous activation of proinflammatory cytokine gene expression. Cell Death Dis. *9*, 500.

STAR★METHODS

KEY RESOURCES TABLE

REAGENT or RESOURCE	SOURCE	IDENTIFIER
Antibodies		
Anti-human caspase-8	MBL	Cat# M058-3, RRID: AB_590761
Anti-cleaved human caspase-3	Cell Signaling Technology	Cat# 9661, RRID: AB_2341188
Anti-human phospho (S358) MLKL	Abcam	Cat# ab187091, RRID: AB_2619685
Anti-human MLKL	Merck Millipore	Cat# MABC604
Anti-GAPDH	Cell Signaling Technology	Cat# 8884s, RRID: AB_11129865
Anti-human CATHEPSIN B	Calbiochem	Cat# IM27L, RRID: AB_2274848
Anti-human CATHEPSIN D	Abcam	Cat# ab75852, RRID: AB_1523267
Anti-rabbit IgG, HRP-linked	Cell Signaling Technology	Cat# 7074, RRID: AB_2099233
Anti-mouse IgG, HRP-linked	Cell Signaling Technology	Cat# 7076, RRID: AB_330924
Bacterial and Virus Strains		
XL1-Blue Competent Cells	Agilent Technologies	200249
Biological Samples		
Buffy Coats	Blood donations to the red cross: "Blutspendedienst des Bayerischen Roten Kreuzes gemeinnützige GmbH"	N/A
Chemicals, Peptides, and Recombinant Proteins		
Recombinant human TNF	ImmunoTools	11343017
Recombinant human GM-CSF	ImmunoTools	21173121
Birinapant	Selleckchem	S7015
Compound A	Gift from Prof. John Silke	N/A
IDN-6556 (Emricasan)	MedChem Express (MCE)	HY-10396
GW280264X	Aobious	AOB3632
Vacuolin	Sigma	673000-10mg
Necrostatin-1	Sigma	N9037-10mg
cOmplete, Mini Protease Inhibitor Cocktail	Sigma	4693159001
Propidium iodide	Sigma	81845
Histopaque-1077	Sigma-Aldrich	10771
Heat inactivated Fetal Bovine Serum	Invitrogen	10270106
Penicillin/Streptomycin	Invitrogen	15140122
RPMI medium	Invitrogen	61870044
Ponceau BS	Sigma	B6008-100 g
Blasticidin	Invivogen	Ant-bl-1
DME medium	Invitrogen	31966047
Serum- and phenolred free media	Thermo Fisher Scientific	11835063
Urea	Sigma	45128-500 g
Thiourea	Sigma	T8656-500 g
Trizma	Sigma	T1503-1kg
Dithiothreitol (DTT)	Sigma	D0632-100 g
Chloroacetamide (CAA)	Sigma	C0267-100 g
Iodoacetamide (IAA)	Sigma	I6125-100 g
Ammonium bicarbonate	Sigma	A6141
Trypsin	Sigma	T6567-1mg
Lys-C	Wako Chemicals	129-02541
DMSO	Sigma	D2650-100ml

(*Continued on next page*)

Continued

REAGENT or RESOURCE	SOURCE	IDENTIFIER
Acetone	Fisher Chemical	67-64-1
Acetonitrile	VWR	20048320
Trifluoroacetic acid	Merck	8082600100
Formic acid	Merck	1002641000
PBS	GIBCO	14190-094
Tween	Acros	233360010
EDTA	Sigma	03677-500 g
Skim milk powder	Roth	T145.3
BSA	Serva	11930.03
Glycerol	Sigma	G5516-1L
Sodium dodecyl sulfate (SDS)	Roth	CN30.3
Sodium deoxycholate (SDC)	Sigma	30970-100 g
Sodium chloride (NaCl)	VWR	27810.295
NuPAGE LDS Sample Buffer (4x)	Invitrogen	NP0007
Igepal	Sigma	I3021-500ml
GelRed nucleic acid stain	Biotium	41003-1
Agarose	Invitrogen	16500-500
RNase A	Thermo Fisher	EN0531
Proteinase K	Thermo Fisher	AM2546
Brefeldin A	Invitrogen	00-4506-51
Puromycin	Invivogen	Ant-pr-5
Polybrene	Sigma	107689
Critical Commercial Assays		
Monocyte isolation kit	Miltenyi Biotec	130-091-153
Human CCL2 Quantikine kit (ELISA)	R&D Systems	DCP00
Human HMGB1 Quantikine kit (ELISA)	Cloud-Clone	ABIN414391
SuperScript III	Invitrogen	11752-050
RNeasy Plus Mini Kit	QIAGEN	74134
QIAshredder	QIAGEN	79656
Deposited Data		
Raw Mass Spectrometry Data Files	This paper	ProteomeXchange Consortium via the PRIDE partner repository, with the dataset identifier PXD014966
Experimental Models: Cell Lines		
U937 cell line	ATCC	CRL-1593.2
293T cell line	ATCC	CRL-3216
Human primary macrophages made out of buffy coats	Blood donation to the Red cross	N/A
Oligonucleotides		
sgRNA 1 against RIPK3: gaattcgtgctgcgcctaga	Tanzer et al., 2017	Metabion
sgRNA 2 against RIPK3: cgccccccttggtgtccatcg	This study	Metabion
Recombinant DNA		
lentiCRISPR v2	Transomics	TELA1002
psPAX2	http://addgene.org/12260	Addgene #122260
pMD2.G	http://addgene.org/12259	Addgene #122259
Software and Algorithms		
MaxQuant	Cox and Mann, 2008, Version 1.5.0.38	https://www.biochem.mpg.de/5111795/maxquant
Perseus	Tyanova et al., 2016, Version 1.5.3.0	https://www.biochem.mpg.de/5111810/perseus

(*Continued on next page*)

Continued

REAGENT or RESOURCE	SOURCE	IDENTIFIER
XCalibur	Thermo Scientific	https://www.thermofisher.com/order/catalog/product/OPTON-30487
Prism Graphpad	N/A	https://www.graphpad.com/scientific-software/prism/
Instant Clue	Nolte et al., 2018	http://www.instantclue.uni-koeln.de/
FlowJo	N/A	https://www.flowjo.com/
R	N/A	https://www.r-project.org/
Adobe Illustrator	N/A	https://www.adobe.com/de/products/illustrator.html?gclid=Cj0KCQiAj4biBRC-ARIsAA4WaFiBQklh92FMEfFeoXKzbZX3ANOyHPWvjWC_Dc8uqRkApS93wRL-0_MaAvthEALw_wcB&sdid=88X75SKP&mv=search&ef_id=Cj0KCQiAj4biBRC-ARIsAA4WaFiBQklh92FMEfFeoXKzbZX3ANOyHPWvjWC_Dc8uqRkApS93wRL-0_MaAvthEALw_wcB:G:s&s_kwcid=AL!3085!3!274277387414!e!!g!!adobe%20illustrator
PRIDE	Jones et al., 2008	https://www.ebi.ac.uk/pride/archive/

LEAD CONTACT AND MATERIALS AVAILABILITY

Further information and requests for resources should be directed to and will be fulfilled by the Lead Contact, Felix Meissner (meissner@biochem.mpg.de). This study did not generate new unique materials and reagents.

EXPERIMENTAL MODEL AND SUBJECT DETAILS

Experiments described in this study are performed with the U937 cell line and human primary macrophages. U937 were purchased at ATCC and cultured in RPMI supplemented with 10% FCS and Pen/Step. Human primary macrophages were generated by isolating PBMCs from buffy coats (generated from blood donations) using Histopaque-1077 (Sigma-Aldrich, 10771). Monocytes were isolated using a monocyte isolation kit (Miltenyi Biotec, 130-091-153), plated and 50 nM GM-CSF (ImmunoTools, 21173121) was added. Cells were left for 7 days to induce macrophage differentiation. All cells were stimulated and kept for the entire treatment duration in serum- and phenol-red free media (Thermo Fisher Scientific, 11835063).

METHOD DETAILS

Sample preparation for proteomic analysis and ELISA of supernatants

1.5×10^6 U937 cells or full 24 wells of primary human macrophages were treated with TNF (30 ng/ml) and the IAP inhibitor, birinapant (SM, 250 nM) (Compound A (2 μM) for human primary macrophages) to induce apoptosis or TNF and birinapant (SM, 250 nM) (Compound A (2 μM) for human primary macrophages) and the caspase inhibitor IDUN-6556 (IDN-6556/emricasan, 10 μM) to induce necroptosis, GW280264X (10 μM, pretreatment for 60 minutes before apoptosis and necroptosis induction), necrostatin-1 (Nec-1, 50 μM), vacuolin-1 (vacuolin, 10 μM) and brefeldin A (BFA, 3 μg/ml, 20 minutes before apoptosis and necroptosis induction). Control cells were treated with DMSO, TNF, birinapant and IDUN-6556 alone. For ELISA supernatants were taken and processed according to the manufacturer's instruction. For proteomic analysis supernatants were spun for 5 minutes at 500 x g to remove cells and filtered through 0.22 μm filters to remove cell debris. 8 M urea in 40 mM HEPES was added to bring the sample to a final concentration of 2.7 M urea, which was subsequently sonicated (Biorupter) for 20 minutes. Proteins were reduced by the addition of 10 mM DTT and incubated for 30 minutes at room temperature. Proteins were alkylated by the addition of 55 mM iodoacetamide and incubated for 20 minutes at room temperature in the dark. 100 mM Thiourea was added before the addition of 1 μg lysC and trypsin and digested over night at room temperature. Enzyme activity was stopped by the addition of 2% ACN and 0.6% TFA and proteins were cleaned up on C18 StageTips (Frauenstein and Meissner, 2018).

Preparation of extracellular vesicles

12×10^6 U937 cells were treated for three hours with TNF and birinapant or TNF and birinapant and IDUN-6556 or with DMSO alone as a control. Cells were spun for 5 minutes at 500 x g. Supernatants were taken and spun again for 30 minutes at 10,000 x g. Supernatants were taken again and spun for 60 minutes at 100,000 x g to obtain extracellular vesicles. The pellets containing extracellular vesicles were washed with ice cold PBS and again centrifuged for 60 minutes at 100,000 x g. Extracellular vesicles were lysed in 8 M Urea with 50 mM Tris (pH8), reduced with 10 mM DTT, alkylated with 40 mM CAA and digested for 2 hours

with lysC (1 μg/sample) before 1:4 dilution with 50 mM ammonium bicarbonate and the addition of trypsin (1 μg/sample). Trypsin and lysC digestion occurred over night at room temperature and peptides were cleaned up by C18 stage tipping.

Western blotting

Two million cells were stimulated, washed in PBS and lysed in buffer (1% IGEPAL, 10% Glycerol, 2 mM EDTA, 50 mM Tris pH 7.5, 150 mM NaCl) supplemented with phosphatase- (Sigma-Aldrich, 4906845001) and protease inhibitors (Sigma-Aldrich, 4693159001). Lysates were kept on ice for 20 minutes and centrifuged at 16,100 x g for 15 minutes before the addition of 6 x SDS sample loading buffer (450 mM Tris-HCl, pH 8, 60% (v/v) glycerol, 12% (w/v) SDS, 0.02% (w/v) bromophenol blue, 600 mM DTT) to the supernatant, followed by boiling and sonication. For immunoblotting of supernatants ten million cells were stimulated in serum-free media, spun down and proteins in supernatants were precipitated with ice-cold Acetone (80% final concentration). The next day precipitates were spun down for 30 minutes at full speed and washed twice in 80% Acetone before addition of 6 x SDS sample loading buffer, boiling and sonication. Separation occurred on 12% Novex Tris-glycine gels (Thermo Fisher Scientific, XP00120BOX) and transferred onto PVDF membranes (Merck Millipore, IPVH00010) or Nitrocellulose membranes (Amersham, 10600002). Membranes were blocked in 5% milk and antibodies diluted in 2% BSA in PBST. Antibodies used for immunoblotting were as follows: anti-human caspase-8 (MBL, M058-3), anti-cleaved human caspase-3 (Cell Signaling, 9661), anti-human phospho (S358) MLKL (Abcam, ab187091), anti-human MLKL (Merck Millipore, MABC604), anti-GAPDH (Cell Signaling Technology, 8884s), anti-CATHEPSIN B (Calbiochem, IM27L) and anti-CATHEPSIN D (Abcam, ab75825).

Cell death analysis

1×10^5 U937 cells and human primary macrophages were plated in 24 well plates and treated with TNF (30 ng/ml), IDN-6556 (10 μM), necrostatin-1 (Nec-1, 50 μM), birinapant (SM, 250 nM) for U937 and Compound A (SM, 2 μM) for human primary macrophages. Cell death was measured by propidium iodide incorporation using flow cytometry (FACS Attune NxT, BD FACS Aria III) and analyzed using Graphpad Prism.

DNA laddering assay

DNA laddering assay was performed as described previously with some changes (Kralj et al., 2003). After stimulation 2×10^6 cells were washed with PBS and lysed in 200 μl of lysis buffer (1% NP-40 in 20 mM EDTA, 50 mM Tris-HCl, pH 7.5), centrifuged at 3000 rpm for 5 min and supernatants were collected. SDS (1%) and RNase A (5 μg/ml) were added for 1 h at 56°C and proteinase K (2.5 μg/ml) was added for 1 h at 37°C. Afterward, ½ volume of ammonium acetate (stock 10 M), 2 volume of ice cold ethanol were added, followed by incubation overnight at −80°C. Samples were centrifuged the next day (14000 rpm) for 40 min at 4°C. Pellets were washed with 70% ethanol and dissolved in 20 μl of water. Equal amounts of DNA were loaded for each condition on a 2% agarose gel.

qPCR

RNA was isolated from 2×10^6 cells with the RNeasy Plus Mini kit (QIAGEN) and reversely transcribed with SuperScript III (Invitrogen). cDNA was amplified with SYBR Green on a Biorad C1000 Thermal Cycler. Primers used were CCL2 (CCCCAGTCACCTGCTGTTAT) and GAPDH (GTCTCCTCTGACTTCAACAGCG). Fold induction compared to untreated controls was calculated by the delta-delta CT method.

Chromatography and mass spectrometry

Samples were loaded onto 50-cm columns packed in-house with C18 1.9 μM ReproSil particles (Dr Maisch GmbH), with an EASY-nLC 1000 system (Thermo Fisher Scientific) coupled to the MS (Q Exactive HF, Thermo Fisher Scientific). A homemade column oven maintained column temperature at 60°C. Peptides were introduced onto the column with buffer A (0.1% Formic acid) and eluted with a 107.3-min gradient of 5 to 25% of buffer B (60% ACN, 0.1% Formic acid), both at a flow rate of 300 nl/min.

A data-dependent acquisition (TopN) MS method was used in which one full scan (300 to 1650 *m/z*, R = 60,000 at 200 *m/z*) at a target of 3×10^6 ions was first performed, followed by 15 data-dependent MS/MS scans with higher energy collisional dissociation [target 10^5 ions, max ion fill time 55 ms, isolation window 1.4 *m/z*, normalized collision energy 27%, R = 15,000 at 200 *m/z*]. Dynamic exclusion of 20 s and apex trigger (4 to 7 s) was enabled.

QUANTIFICATION AND STATISTICAL ANALYSIS

MS raw files were processed by the MaxQuant software version 1.5.0.38 (Cox and Mann, 2008) and fragments lists were searched against the human Uniprot Reference Proteome without isoforms (August 2015) by the Andromeda search engine (Cox et al., 2011) with cysteine carbamidomethylation as a fixed modification and N-terminal acetylation and methionine oxidations as variable modifications. We set the false discovery rate (FDR) to 0.01 at the peptide and protein levels and specified a minimum length of 7 amino acids for peptides. Enzyme specificity was set as C-terminal to Arginine and Lysine as expected using Trypsin and LysC as proteases and set as semi-tryptic for semi-tryptic peptide analysis, and a maximum of two missed cleavages.

All bioinformatics analyzes were done with the Perseus software (version 1.5.3.0) (Tyanova et al., 2016) of the MaxQuant computational platform. Quantified proteins are filtered for at least 75% of valid values among three or four biological replicates in at least one condition. Missing values were imputed and significantly up- or downregulated proteins were determined by multiple-sample test (FDR = 0.05) and Student's t test (two-sided), (FDR = 0.05). n represents replicates of the same cell line stimulated separately. Further statistical details of experiments can be found in the figure legends.

The 1D annotation enrichment analysis detects whether expression values of proteins belonging to an enrichment term (here we used: keywords, GOCC, GOMF, GOBP and KEGG name) show a systematic enrichment or de-enrichment compared to the distribution of all expression values (Cox and Mann, 2012).

Swarm plots were created using the software Instant Clue (Nolte et al., 2018).

DATA AND CODE AVAILABILITY

The MS-based proteomics data have been deposited to the ProteomeXchange Consortium via the PRIDE partner repository and are available via ProteomeXchange with identifier (PXD014966) (Jones et al., 2008).